EFFECT OF IMPURITIES IN CO_2 AT SUPERCRITICAL PRESSURE ON ALLOY COMPATIBILITY

B. A. Pint and J. R. Keiser
Oak Ridge National Laboratory, Oak Ridge, TN USA

ABSTRACT

Direct-fired supercritical CO_2 (sCO_2) cycles are expected to result in sCO_2 with higher impurity levels compared to indirect-fired cycles. Prior work at ambient pressure showed minimal effects of O_2 and H_2O additions, however, a new experimental rig has been built to have flowing controlled impurity levels at supercritical pressures at ≤800°C. Based on industry input, the first experiment was conducted at 750°C/300 bar in CO_2+1%O_2-0.25%H_2O using 500-h cycles for up to 5,000 h. Compared to research grade sCO_2, the results indicate faster reaction rates for Fe-based alloys like 310HN and smaller increases for Ni-based alloys like alloys 617B and 282. It is difficult to quantify the 310HN rate increase because of scale spallation. Characterization of the 5,000 h specimens indicated a thicker reaction product formed, which has not been observed in previous impurity studies at ambient pressure. These results suggest that more studies of impurity effects are needed at supercritical pressures including steels at lower temperatures.

INTRODUCTION

While supercritical CO_2 (sCO_2) cycles offer attractive features for a range of power generation applications [1-3], the revolutionary aspect of sCO_2 is the direct-fired or open cycle [4-5], which has the potential to achieve economical, "clean" fossil energy power generation by diverting a portion of the CO_2 at the bottom of the cycle for sequestration or enhanced oil recovery. A pilot plant using the Allam cycle [4,5] is now being tested in Texas. However, the combustion of natural gas or coal-derived synthesis gas would incorporate high levels of impurities (e.g. H_2O, O_2, etc.) into the supercritical fluid. It is now well-accepted that Ni-based alloys have reasonable compatibility with sCO_2 at up to 800°C [6-12]. However, impurity effects at supercritical pressures have not been well-studied and the effects of O_2 and H_2O are not resolved [12-14]. A new experimental rig was recently constructed and the first set of experiments was completed at 750°C/300bar with 1%O_2 and 0.25%H_2O additions [12]. This paper provides additional characterization from the 5,000 h specimens including Fe- and Ni-based alloys. For applications above 700°C, precipitation-strengthened (PS) Ni-based alloys, such as 740 and 282 [15,16], are needed. These impurity levels at 300 bar increased the specimen mass change, particularly for the Fe-based alloys.

EXPERIMENTAL PROCEDURE

Table 1 provides the measured composition of the alloys, which were machined into coupons typically 1.5 x 12 x 20 mm and polished to a 600 grit surface finish on all sides. Prior to exposure, the coupons were ultrasonically cleaned in acetone and methanol. All exposures used 500-h cycles at 750°C. For the 1 bar exposures in laboratory air or research grade (RG) CO_2 (measured 4.1±0.7 ppm H_2O, and <5 ppm total hydrocarbons specified), the specimens were held in pre-annealed alumina boats. For the laboratory air (~50% relative humidity) exposures, the specimens were slowly heated to temperature (~4 h) in a resistively heated box furnace, held for 500-h and then furnace cooled to room temperature. For CO_2, the specimens were slowly heated to temperature in Ar over several hours (~2°C/min) in a horizontal alumina tube with end caps within a 3-zone furnace. The specimens were held at temperature ±2°C for 500 h in the flowing gas (100 cc/min at 25°C) and then cooled in Ar to room temperature inside the furnace. For the 300 bar exposures, the experiments were conducted in a vertically-oriented, alloy 282 autoclave (~266 mm x 83 mm inner diameter) described previously [8,9]. Specimens were held on an alloy 282 sample rack and slowly heated to temperature over several hours (~2°C/min) in sCO_2 flowing at ~ 2 cc/min, held at temperature ±2°C and then cooled in sCO_2 to room temperature using a cooling fan. One autoclave was modified to use two pumps to deliver sCO_2, CO_2-O_2 and H_2O. Based on the gas flow rate, the O_2 level was calculated as 1.0±0.2% and the H_2O content as 0.25±0.05% for the high impurity experiment. For all of the experiments, mass change was measured using a Mettler Toledo model XP205 balance (±0.04 mg accuracy or ±0.01 mg/cm^2). After exposure, specimens were Cu-plated to protect the surface oxide and metallographically mounted and imaged with light microscopy. Oxide thickness was measured using image analysis software with ~20-30 measurements taken for each specimen. Specimens were examined using a Hitachi model S4800 scanning electron microscope (SEM) with EDS detector.

RESULTS & DISCUSSION

Figure 1 shows the median mass change data at 750°C/300 bar for 3-5 specimens exposed to RG sCO_2 (dashed lines) and RG sCO_2 with 1%O_2 and 0.25%H_2O (solid lines and boxes) [12]. The mass gains were much higher for some materials such as 247 and 310HN, which also exhibited scale spallation. Specimens were inserted in the 2nd and 3rd cycles that were removed after 2,500 and 1,000 h exposures, respectively. In some cases, such as the 617B and 247 specimens, these specimens gained more mass than the three specimens exposed for 5,000 h.

Table 1. Chemical compositions (mass%) determined by inductively coupled plasma analysis and combustion analysis

Material	Fe	Ni	Cr	Al	S	Other
25	42.6	25.4	22.3	0.03	0.0008	3.4W,3.0Cu,1.5Co,0.5Mn,0.5Nb,0.2Si,0.2N
310HN	51.3	20.3	25.5	<	0.0006	0.3Co,0.4Nb,1.2Mn,0.3Si,0.3N,0.05C
625	4.0	60.6	21.7	0.09	0.0010	9.4Mo,3.6Nb,0.2Ti,0.2Si,0.1Mn
617B	1.2	54.6	22.3	1.0	<0.001	11.9Co,8.2Mo,0.4Ti,0.05Si,0.04Mn,0.005B
230	1.5	60.5	22.6	0.3	0.0009	12.3W,1.4Mo,0.5Mn,0.4Si
740	1.9	48.2	23.4	0.8	0.0006	20.2Co,2.1Nb,2.0Ti,0.3Mn,0.5Si
282	0.2	58.0	19.3	1.5	<0.0001	10.3Co,8.3Mo,0.06Si,2.2Ti,0.1Mn
247	0.07	59.5	8.5	5.7	<0.0003	9.8Co,9.9W,0.7Mo,3.1Ta,1.0Ti,1.4Hf

< indicates less than 0.01%

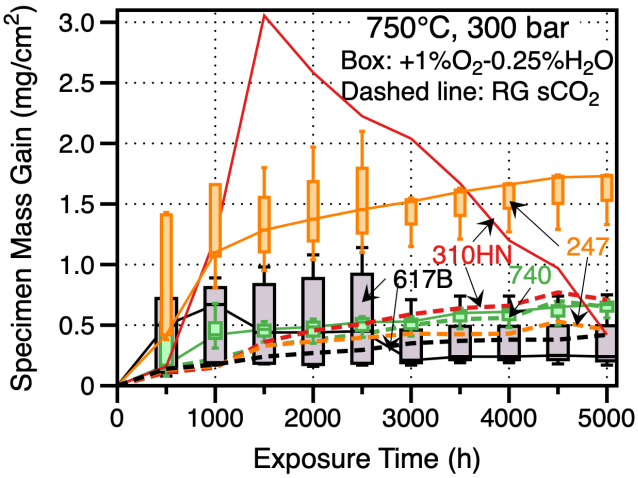

Figure 1: Median specimen mass gain data for 500-h cycles at 750°C in 300 bar RG sCO_2 (dashed lines) and RG sCO_2 with 1% O_2 and 0.25% H_2O (solid lines). Box and whisker plots show data for 3-5 specimens exposed in the high impurity environment [12].

To summarize the results for all of the alloys studied, Fig. 2 shows median mass change results for each of the alloys exposed at 750°C for 5,000 h. For comparison, median mass change results are shown for laboratory air and 1 bar RG CO_2. The 1 bar results put the 300 bar results into better context. Many of the Ni-based alloys showed no effect of the exposure in impure sCO_2. The mass gains are consistently higher for the PS alloys 740 and 282 because of the higher Ti contents (Table 1) accelerating growth of the Cr-rich oxide [17,18]. The materials most strongly affected by the impurity additions were the alumina-forming superalloy 247 and the Fe-based alloys 25 and 310HN. The latter did not show a high mass gain because of scale spallation, Fig. 1.

Figure 3 compares the reaction products formed on four alloys after 5,000 h in the four environments shown in Fig. 2: laboratory air, 1 bar RG CO_2, 300 bar RG sCO_2 and 300 bar RG sCO_2 with 1%O_2 and 0.25%H_2O. In most cases, the reaction products were thin, even for the

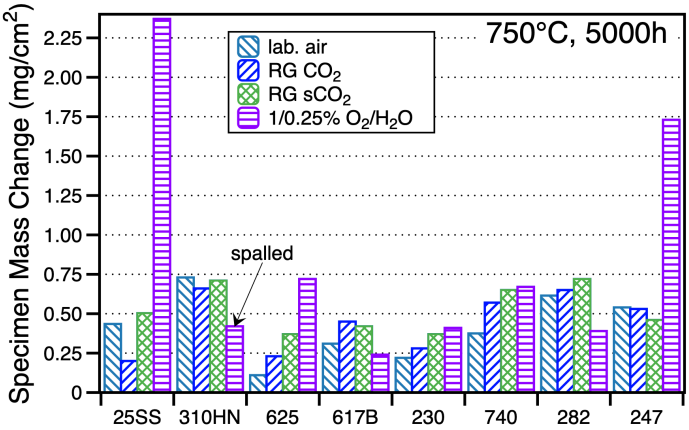

Figure 2: Median specimen mass gain values after 5,000 h exposures at 750°C in three different environments compared to laboratory air exposures.

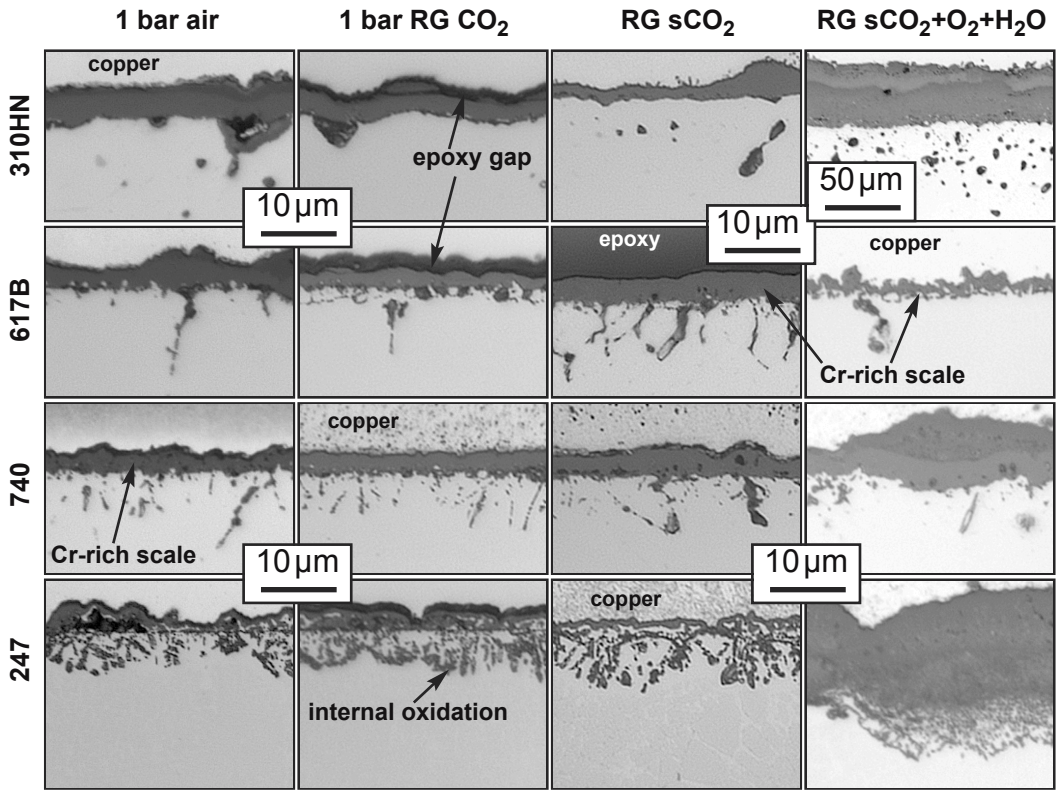

Figure 3: Light microscopy of polished cross-sections of specimens exposed for 5,000 h at 750°C in four different environments.

stainless steel, 310HN. The exceptions were in the high impurity sCO_2 environment where much thicker oxides were observed on several alloys, consistent with the mass gains in Figs. 1 and 2. The major increase for the 310HN specimen required a different magnification in Fig. 3. The Ni-based alloys all showed significant internal oxidation that increased in volume with Al and Ti contents, Table 1. While 247 can form alumina in some conditions, this temperature is too low to form alumina even in air. With the addition of impurities, there was a significant increase in the oxide formed on the 247 specimen. The other alloys also formed thicker oxides, except for the 617B specimen. Figure 1 also shows a lower mass gain with the addition of impurities for the 617B specimens.

To quantify results from multiple images of each specimen, Figure 4 shows oxide thickness measurements for several alloys as a function of exposure time at 750°C in three different environments. For 310HN, thin oxides were measured for 1 and 300 bar RG sCO_2 that were slightly increasing with exposure time. In contrast, a dramatic increase in oxide thickness was observed with the addition of impurities at 300 bar. The effect of impurities was less dramatic for the other Ni-based alloys shown in Fig. 4. The one exception was that the oxide was thinner for the high impurity case for the 617B and 282 specimens exposed for 5,000 h. Further studies are needed to explain this somewhat unusual result. It may be due to a variability in the experimental conditions.

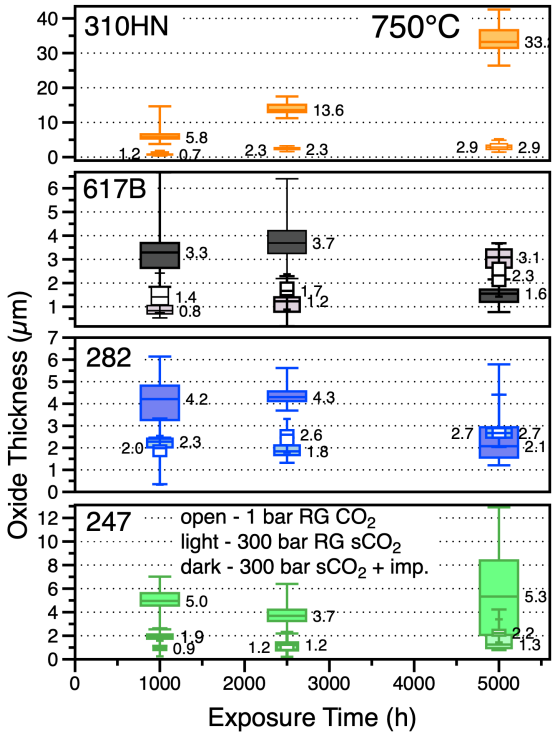

Figure 4: Box and whisker plots of oxide thickness for alloy 310HN, 617B, 282 and 247 specimens exposed at 750°C in 1 and 300 bar RG sCO_2 and 300 bar CO_2+1%O_2+0.25%H_2O.

Previously, SEM characterization of specimens of alloys 25 and 247 exposed for 1,000 h were presented [12]. Figures 5-8 show comparisons of 310HN and 282 after 5,000 h exposures in RG sCO_2 with and without impurity additions. Figure 5 shows the relatively thin and compact Cr-rich oxide formed on the 310HN specimen in RG sCO_2. The outer part of the scale contains Mn and an inner Si-rich layer is typical for steels at this temperature, Figs. 5b and 5d. The Nb-rich strengthening precipitates are shown in Fig. 5f. A relatively thin area of oxide was found for imaging after exposure to the high impurity environment, Figure 6. In this case, some Fe was found in the outer scale above the Cr-rich inner layer, Fig. 6f. Otherwise the oxide was similar to that formed in RG sCO_2. It is possible that this region spalled during the 10 thermal cycles.

Figure 7 shows the more complex scale formed on 282 after 5,000 h in RG sCO_2. While primarily a Cr-rich oxide, Figs. 7c and 7e, Ti-rich precipitates were observed at the gas and metal-scale interfaces, Fig. 7d. Also, Al was observed to internally oxidize, Fig. 7f, and Mo was enriched in areas where Cr was depleted, Fig. 7b. These are similar observations to prior TEM characterization after 1,000 h at 750°C in industrial grade sCO_2 [19]. Figure 8 shows a region that was slightly thicker than average for characterization after exposure to the high impurity environment. Similar to Fig. 7, a Cr-rich oxide with Ti-rich precipitates and Al-rich internal oxidation was observed, Fig. 8. But in this region an outer Co-containing oxide nodule formed,

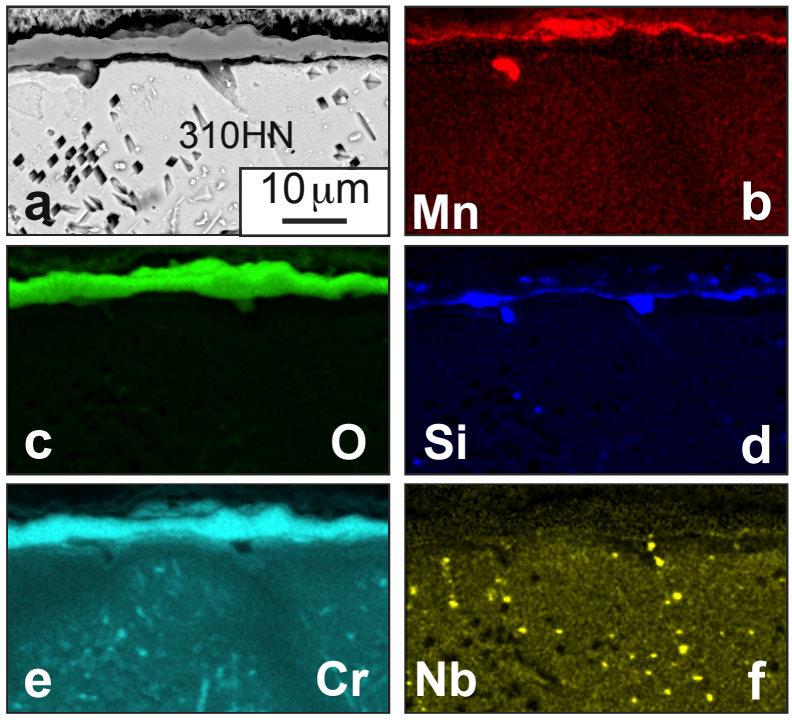

Figure 5. (a) SEM secondary electron image of the scale formed on alloy 310HN after 5,000 h at 750°C in 30 MPa RG sCO_2 and associated EDS maps (b) Mn, (c) O, (d) Si, (e) Cr and (f) Nb.

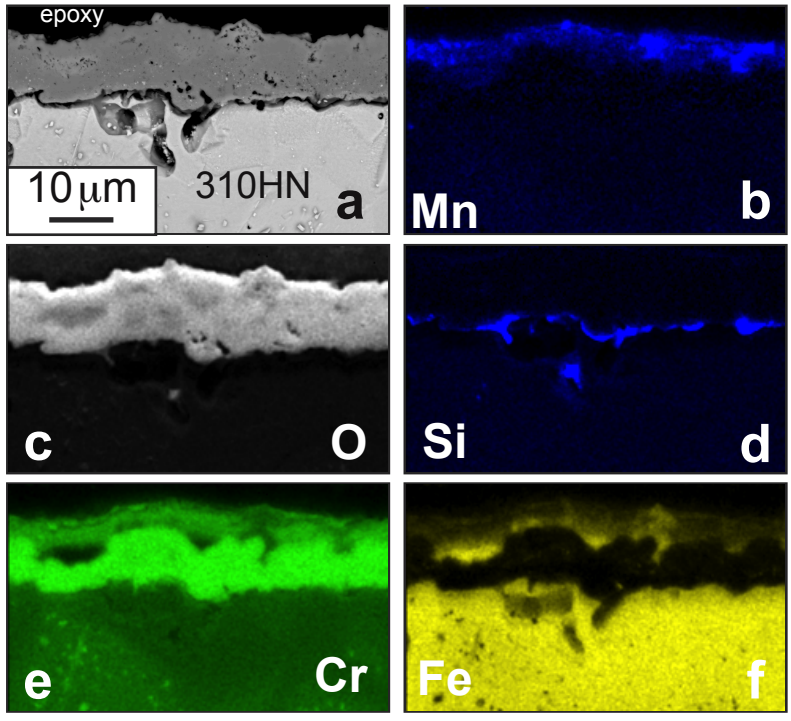

Figure 6. (a) SEM secondary electron image of the scale formed on alloy 310HN after 5,000 h at 750°C in 30 MPa sCO_2+1%O_2+0.25%H_2O and associated EDS maps (b) Mn, (c) O, (d) Si, (e) Cr and (f) Fe.

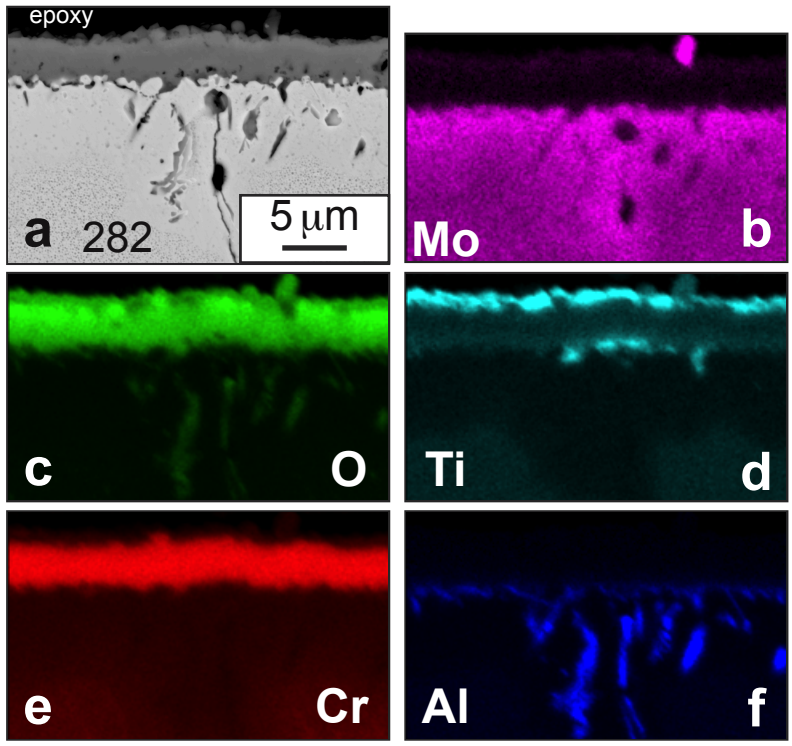

Figure 7. (a) SEM secondary electron image of the scale formed on alloy 282 after 5,000 h at 750°C in 30 MPa RG sCO_2 and associated EDS maps (b) Mo, (c) O, (d) Ti, (e) Cr and (f) Al.

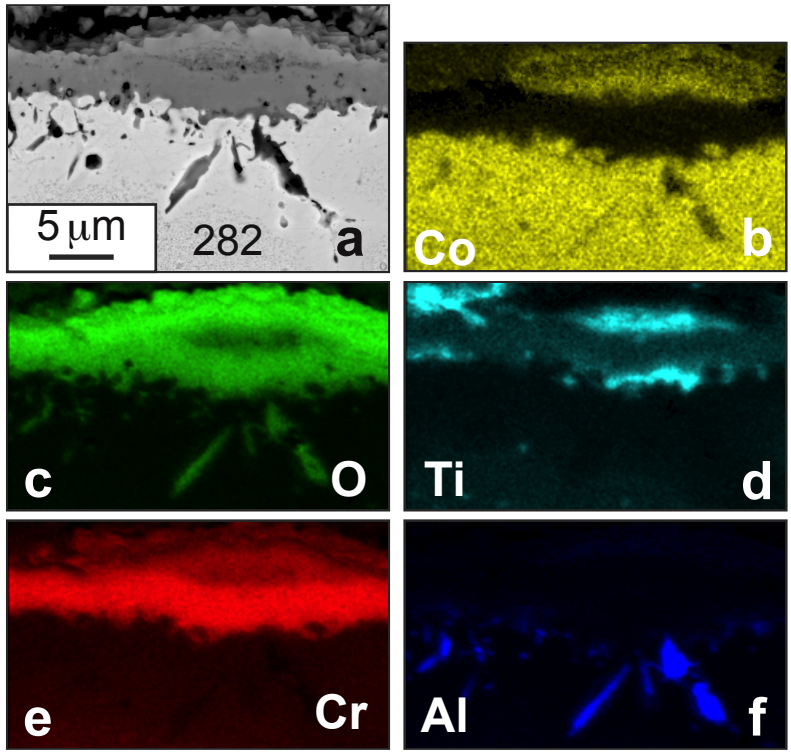

Figure 8. (a) SEM image of the scale formed on alloy 310HN after 5,000 h at 750°C in 30 MPa sCO_2+1%O_2+0.25%H_2O and associated EDS maps (b) Co, (c) O, (d) Ti, (e) Cr and (f) Al.

SUMMARY AND FUTURE PLANS

Impurities in direct-fired supercritical CO_2 (sCO_2) cycles are a significant concern for long-term compatibility. For the first exposure in a new experimental rig, a 5,000 h exposure was performed at 750°C in CO_2+1%O_2-0.25%H_2O using 500-h cycles. For comparison, similar exposures were conducted in laboratory air, 1 bar RG CO_2 and 300 bar RG sCO_2. Commercial Fe- and Ni-base structural alloys were exposed in each environment and reaction products were characterized. With the addition of controlled levels of impurities, the Fe-based alloys appeared to be more strongly affected. Most Ni-based alloys were not affected by the addition of impurities. For lower temperatures, where steels are more likely structural alloy candidates, additional work is needed to further understand the role of impurities on sCO_2 compatibility. In order to determine a better mechanistic understanding, additional experiments are needed where only O_2 or H_2O is added.

ACKNOWLEDGMENTS

The experimental work at ORNL was conducted by M. Howell, M. Stephens, T. Lowe and T. Jordan. Material was provided by Haynes International, Special Metals, Capstone Turbines, Sandvik and VDM. S. S. Raiman and M. J. Lance provided useful comments on the manuscript. Research sponsored by the U. S. Department of Energy, Office of Fossil Energy, Coal and Power R&D. This manuscript has been authored by UT-Battelle, LLC under Contract No. DE-AC05-00OR22725 with the U.S. Department of Energy. The United States Government retains and the publisher, by accepting the article for publication, acknowledges that the United States Government retains a non-exclusive, paid-up, irrevocable, world-wide license to publish or reproduce the published form of this manuscript, or allow others to do so, for United States Government purposes. The Department of Energy will provide public access to these results of federally sponsored research in accordance with the DOE Public Access Plan (http://energy.gov/downloads/doe-public-access-plan).

REFERENCES

1. Chen, H., Goswami, D. Y., Stefanakos, E. K., "A review of thermodynamic cycles and working fluids for the conversion of low-grade heat," *Renewable & Sustainable Energy Reviews*, Vol. 14, (2010), pp.3059-3067.
2. Dostal, V., Hejzlar, P., Driscoll, M. J., "High-Performance Supercritical Carbon Dioxide Cycle for Next-Generation Nuclear Reactors," *Nuclear Technology*, Vol. 154, No.3 (2006), pp. 265-282.
3. Iverson, B. D., Conboy, T. M., Pasch, J. J., Kruizenga, A. M., "Supercritical CO_2 Brayton cycles for solar-thermal energy," *Applied Energy*, Vol. 111, (2013), pp. 957-970.
4. Allam, R. J., Palmer, M. R., Brown Jr., G. W., Fetvedt, J., Freed, D., Nomoto, H., Itoh, M., Okita, N., Jones Jr., C., "High efficiency and low cost of electricity generation from fossil fuels while eliminating atmospheric emissions, including carbon dioxide," *Energy Procedia*, Vol. 37, (2013), pp. 1135-1149.
5. Wright, I. G., Pint, B. A., Shingledecker, J. P., Thimsen, D., (2013) "Materials Considerations for Supercritical CO_2 Turbine Cycles," ASME Paper #GT2013-94941, presented at the International Gas Turbine & Aeroengine Congress & Exhibition, San Antonio, TX, June 2013.
6. Firouzdor, V., Sridharan, K., Cao, G., Anderson, M., Allen, T. R., "Corrosion of a stainless steel and nickel-based alloys in high temperature supercritical carbon dioxide environment," *Corrosion Science*, Vol. 69, (2013), pp. 281-291.

7. Olivares, R. I., Young, D. J., Marvig, P., Stein, W., "Alloys SS316 and Hastelloy-C276 in Supercritical CO_2 at High Temperature," *Oxidation of Metals*, Vol. 84, (2015), pp. 585–606.
8. Pint, B. A., Keiser, J. R., "Initial Assessment of Ni-Base Alloy Performance in 0.1 MPa and Supercritical CO_2," *JOM*, Vol. 67, No.11 (2015), pp. 2615-2620.
9. Pint B. A., Brese, R. G., Keiser, J. R., "Effect of Pressure on Supercritical CO_2 Compatibility of Structural Alloys at 750°C," *Materials and Corrosion*, Vol. 68, (2017), pp. 151-158.
10. Olivares, R. I.., Young, D. J., Nguyen T. D., Marvig, P., "Resistance of High-Nickel, Heat-Resisting Alloys to Air and to Supercritical CO_2 at High Temperatures," *Oxidation of Metals*, Vol. 90, (2018), pp. 1-25.
11. Pint, B. A., Keiser, J. R., "Effect of Pressure and Thermal Cycling on Long-Term Oxidation in Supercritical CO_2," NACE Paper C2019-12750, Houston, TX, presented at NACE Corrosion 2019, Nashville, TN, March 2019.
12. Pint, B. A., Lehmusto, J., Lance, M. J., Keiser, J. R., "The Effect of Pressure and Impurities on Oxidation in Supercritical CO_2," *Materials and Corrosion*, in press (2019).
13. Kung, S. C., Shingledecker, J. P., Thimsen, D., Wright, I. G., Tossey, B. M., Sabau, A. S., "Oxidation/Corrosion in Materials for Supercritical CO_2 Power Cycles," in Proceedings of the 5th International Symposium on Supercritical CO_2 Power Cycles, San Antonio, TX, March 2016, Paper #9.
14. Mahaffey, J., Schroeder, A., Adam, D., Brittan, A., Anderson, M., Couet, A., Sridharan, K.,"Effects of CO and O_2 Impurities on Supercritical CO_2 Corrosion of Alloy 625," *Metallurgical and Materials Transactions A*, Vol. 49, (2018), pp. 3703-3714.
15. Pike, L. M., "Development of a Fabricable Gamma-Prime (γ') Strengthened Superalloy," in *Superalloys 2008*, R. C. Reed et al. eds, TMS, Warrendale, PA, 2008, pp. 191-200.
16. Shingledecker J. P., Pharr, G. M., "Testing and Analysis of Full-Scale Creep-Rupture Experiments on Inconel Alloy 740 Cold-Formed Tubing," *J. Mater. Eng. Performance*, Vol. 22, (2013), pp. 454-462.
17. Ennis P. J., Quadakkers, W. J., "Corrosion and Creep of Nickel-Base Alloys in Steam Reforming Gas," in *High Temperature Alloys, Their Exploitable Potential*, eds. J. B. Marriott, M. Merz, J. Nihoul and J. Ward, Elsevier, London, 1985, pp.465-474.
18. Brady, M. P., Pint, B. A., Lu, Z. G., Zhu, J. H., Milliken, C. E., Kreidler, E. D.. Miller, L., Armstrong, T. R., Walker, L. R., "Comparison of Oxidation Behavior and Electrical Properties of Doped NiO- and Cr_2O_3-Forming Alloys for Solid Oxide Fuel Cell Metallic Interconnects," *Oxidation of Metals*, Vol.65, (2006), pp.237-261.
19. Pint, B. A., Unocic, K. A., Brese, R. G., Keiser, J. R., "Characterization of Chromia Scales Formed in Supercritical Carbon Dioxide," *Materials at High Temperature*, Vol. 35, (2018), pp. 39-49.